Journal of Alloys and Compounds 501 (2010) L15–L19

Contents lists available at ScienceDirect

Journal of Alloys and Compounds

journal homepage: www.elsevier.com/locate/jallcom

Letter

Biomolecule-assisted synthesis of Ag_3SbS_3 nanorods

Jiasong Zhong[a], Jie Hu[b], Wen Cai[b], Fan Yang[a], Lijun Liu[a], Haitao Liu[a], Xinyu Yang[a], Xiaojuan Liang[a], Weidong Xiang[a,b,*]

[a] College of Chemistry and Materials Engineering, Wenzhou University, Wenzhou 325035, PR China
[b] College of Materials Science and Engineering, Tongji University, Shanghai 200092, PR China

ARTICLE INFO

Article history:
Received 10 March 2010
Received in revised form 6 April 2010
Accepted 8 April 2010
Available online 20 April 2010

Keywords:
Ag_3SbS_3
L-Cystine
Nanostructured materials
Chemical synthesis
X-ray diffraction

ABSTRACT

A novel biomolecule-assisted method has been successfully developed to prepare pyrargyrite (Ag_3SbS_3) nanorods via the reactions between $AgNO_3$ and $SbCl_3$ with L-cystine in ethylene glycol at 200 °C for 15 h, in which L-cystine was used as the sulfide source and complexing agent. The crystal phase, morphology, grain size, and chemical composition of the as-prepared products were characterized in detail by X-ray powder diffraction (XRD), energy dispersion spectroscopy (EDS), X-ray photoelectron spectroscopy (XPS), field-emission scanning electron microscopy (FESEM), transmission electron microscopy (TEM), and high-resolution transmission electron microscopy (HRTEM). Results revealed that the as-synthesized Ag_3SbS_3 nanorods had diameters range from 150 to 200 nm and lengths up to several micrometers. The experimental results showed that the reaction time played an important role in the formation of Ag_3SbS_3 nanocrystalline. A possible formation mechanism for Ag_3SbS_3 nanorods was discussed.

1. Introduction

In the past few decades, inorganic nanocrystals with controlled size and shape have drawn much attention in both fields of science and technology due to their unique properties and potential applications in nanodevices [1–3]. In particular, semiconductor nanomaterials have been of great interest because of their optical and electrical properties, which may be widely used in the area of optoelectronics [4–6]. Among all these semiconductors, chalcogenide semiconductor materials have driven extensive research interest for various device applications such as linear or nonlinear optoelectronic, and thermoelectric devices as well as optical recording media [7–9]. Moreover, chalcogenide semiconductor materials are attracting special interest from materials scientists and information recording specialists due to the unique possibility of optical information storage [10]. As an important part of chalcogenide semiconductor materials, pyrargyrite (Ag_3SbS_3) is an attractive substance for different optoelectronic and data storage applications [11]. Being promising materials with potential applications, they can be prepared in a variety of ways, such as solvothermal [12] and polyol method [13]. However, it is still a great challenge to develop a simple, inexpensive, environment-friendly and reliable synthetic route to synthesize Ag_3SbS_3 nanomaterials.

It is known that biomolecules, as life's basic building blocks, have special structures and fascinating self-assembling functions, which make them act as templates for the design and synthesis of complicated structures [14]. Based on these facts, biomolecule-assisted synthesis has attracted more and more attention in recent years in the preparation of inorganic materials. Biomolecule-assisted synthesis has been proven to be a novel, environment-friendly, and promising method in the preparation of various nanomaterials owing to its convenience and strong function in morphology control [15]. Many kinds of biomolecules such as DNA [16], protein [17], glutathione [18,19], virus [20], glycine [21], β-carotene [22] and L-cysteine [23,24] have been extensively utilized as templates for the fabrication of inorganic materials with complicated structures [25]. Inspired by their work, it is interesting to investigate other biomolecules to synthesize inorganic materials with desired shape or complicated structures via biomolecules-assisted approaches. L-Cystine ($C_6H_{12}N_2O_4S_2$) is an inexpensive, simple, and environment-friendly thiol-containing amino acid, which had been extensively applied in medicine, foodstuff, cosmetic, etc. To the best of our knowledge, there have been no reports on the synthesis of Ag_3SbS_3 nanocrystalline with L-cystine as the sulfur source to date. Herein, a facile L-cystine assisted approach has been developed to synthesize Ag_3SbS_3 nanocrystalline under solvothermal conditions, in which L-cystine is used as the sulfide source and complexing agent. Emphatically, no nauseous scent (H_2S) appeared in our experiments. The formation mechanism for Ag_3SbS_3 nanocrystalline is presented. This novel and environment-friendly biological technique based on L-cystine can be extended to fabricate other ternary chalcogenide semiconductor materials.

* Corresponding author at: College of Chemistry and Materials Engineering, Wenzhou University, Wenzhou 325035, PR China.
Tel.: +86 577 86596013; fax: +86 577 86689644.
E-mail address: weidongxiang@yahoo.com.cn (W. Xiang).

0925-8388/$ – see front matter © 2010 Elsevier B.V. All rights reserved.
doi:10.1016/j.jallcom.2010.04.070

2. Experimental

2.1. Ag_3SbS_3 nanorods preparation

All of the chemicals were analytical grade and used without further purification. In a typical experiment, analytically pure $AgNO_3$ (3 mmol), $SbCl_3$ (1 mmol) and L-cystine (3 mmol) were dissolved in 40 ml ethylene glycol under constant stirring. Appropriate amount of HCl (2 mol/L) was added into the above solution mixture drop by drop to get a homogeneous solution. Then the obtained solution was transferred into a Teflon-lined stainless-steel autoclave with a capacity of 50 ml. The autoclave was sealed and maintained at 200 °C for 15 h and then cooled to room temperature naturally. The rosy precipitate was collected and washed several times with distilled water and absolute alcohol, respectively. Then, the samples were dried in a vacuum at 60 °C for 4 h.

2.2. Characterization

X-ray powder diffraction (XRD) analysis was carried out on a Bruker D8 Advance diffractometer (40 kV, 40 mA) using Cu Kα radiation (λ = 0.15406 nm) in the 2θ angular range of 10–70° at a scanning rate of 0.02°/s and X-ray photoelectron spectra (XPS) analysis was performed on a AXIS ULTRA DLD X-ray photoelectron spectrometer, using Monochrome Al Ka as the excitation source. The morphology of the samples was studied by field-emission scanning electron microscope (FESEM) on a JEOL instrument (JEOL-6700F) at an accelerating voltage of 10 kV. Energy dispersive spectrometry (EDS) analysis of the product was carried out on an OXFORD INCA instrument attached to the scanning electron microscopy in the scanning range of 0–20 kV. The microstructure and morphologies of the samples were also obtained from transmission electron microscopy (TEM) images and high-resolution TEM (HRTEM) images were recorded on a FEI Tecnai F-20 transmission electron microscopy at an acceleration voltage of 200 kV. All the measurements were carried out at room temperature.

3. Results and discussion

The crystal structure and phase composition of the resulting sample are characterized using X-ray powder diffraction (XRD) technique. Fig. 1 displays the typical XRD pattern of the Ag_3SbS_3 sample obtained at 200 °C for 15 h. All the peaks can be indexed to the hexagonal phase of Ag_3SbS_3. The cell constants are calculated to be $a = 11.039$ Å and $c = 8.715$ Å, which are close to the reported values ($a = 11.047$ Å and $c = 8.719$ Å) for Ag_3SbS_3 phase in the JCPDS card (no. 21-1173). No other diffraction peaks of impurities, such as Sb_2S_3, Ag_2S and Sb_2O_3 are observed in the XRD pattern, which indicates that pure Ag_3SbS_3 has been obtained under the current synthesis conditions.

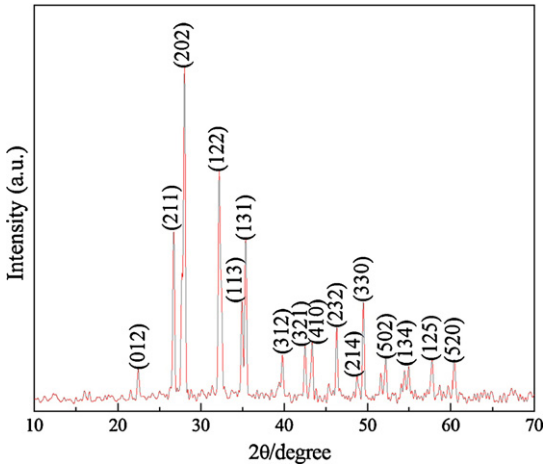

Fig. 1. Typical XRD pattern of as-prepared Ag_3SbS_3 synthesized at 200 °C for 15 h.

The composition and purity of the as-synthesized Ag_3SbS_3 nanorods are further investigated by XPS. The Ag3d core level spec-

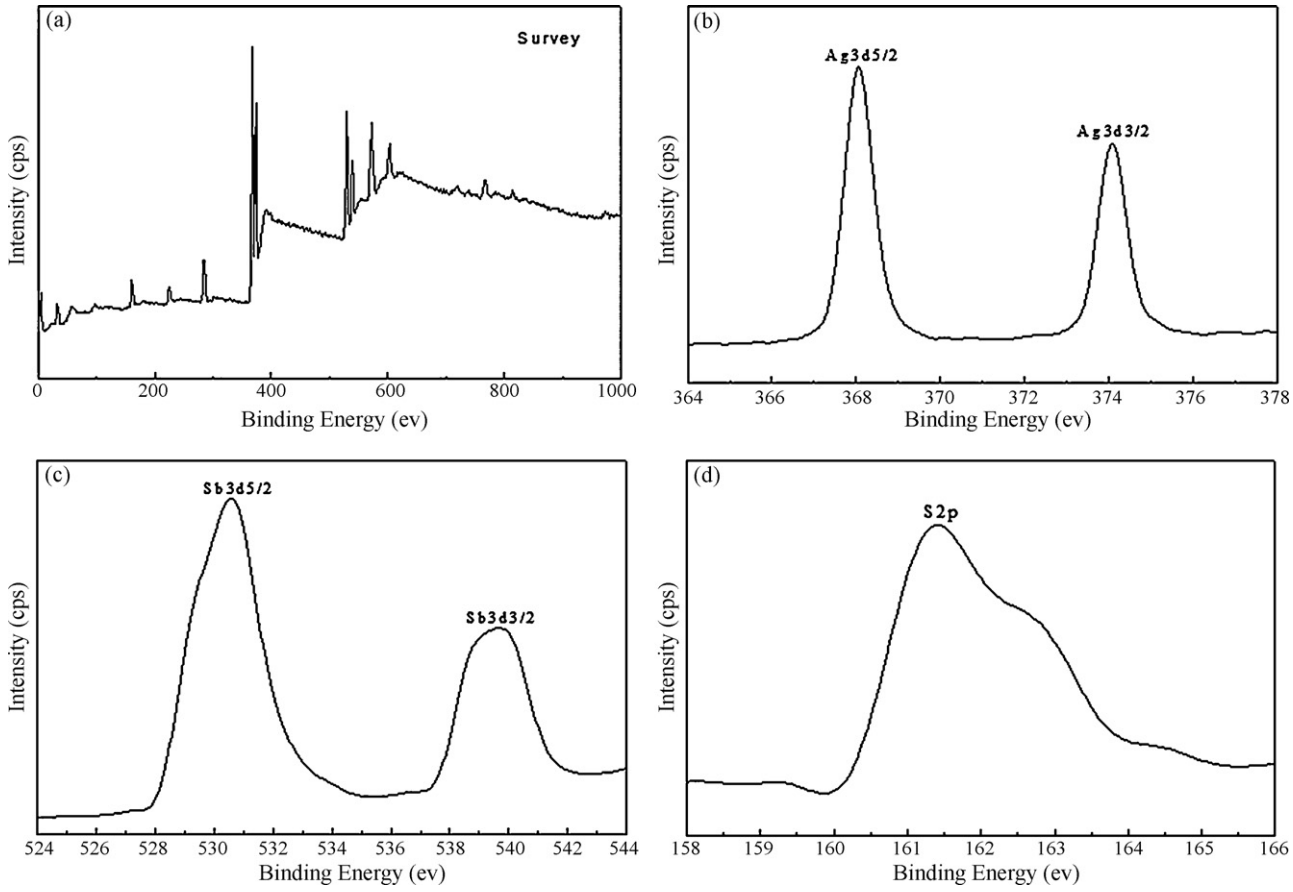

Fig. 2. XPS spectra of the Ag_3SbS_3 product: (a) typical XPS survey spectrum of the Ag_3SbS_3 product, (b) core level spectrum for Ag3d, (c) core level spectrum for Sb3d, and (d) core level spectrum for S2p.

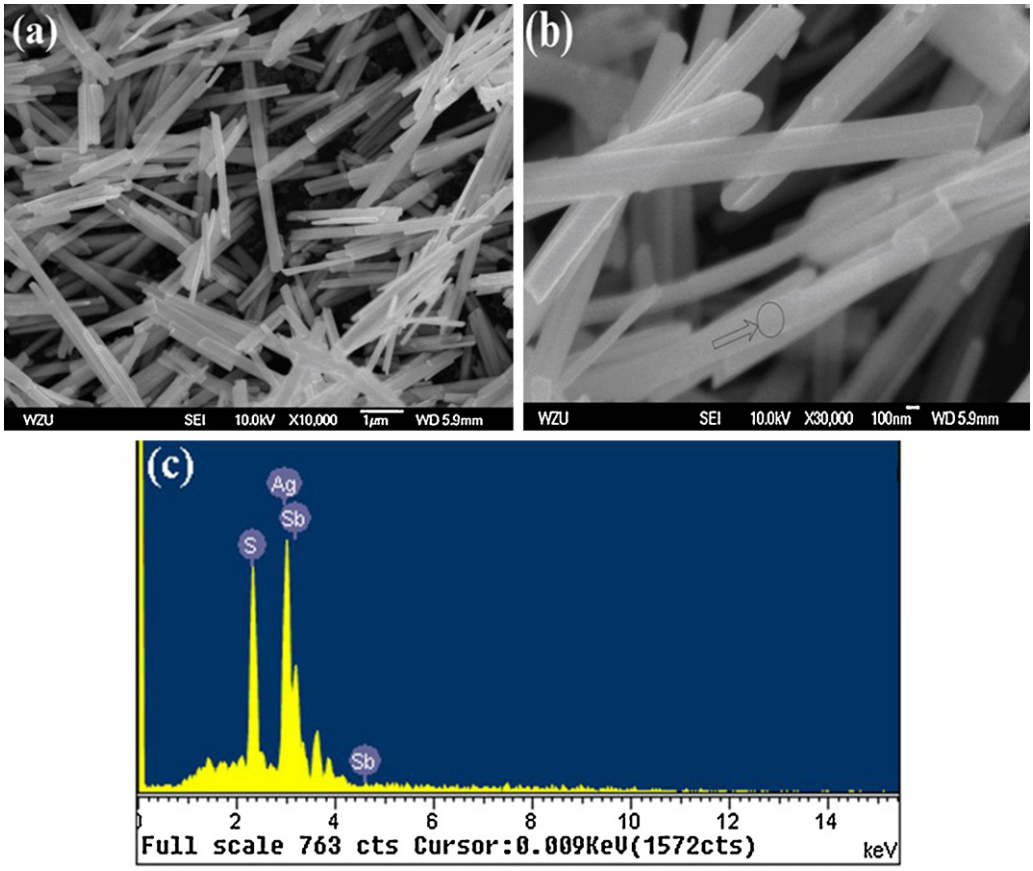

Fig. 3. (a) The FESEM images of Ag_3SbS_3 products, (b) an enlarged FESEM image of (a) and (c) EDS spectrum of a single nanorod (the EDS pattern is obtained from the black circular area demarcated in (b)).

trum is shown in Fig. 3b, indicating that the observed values of the binding energies for $Ag3d_{5/2}$ and $Ag3d_{3/2}$ peaks are 368.05 and 374.07 eV, respectively. Fig. 2c is the typical Sb3d core level spectrum, showing that the strong peak at 530.58 and 539.68 eV corresponds to the Sb3d binding energy for Ag_3SbS_3. The S2p core level spectrum (Fig. 2d) shows a peak located at 161.51 eV. All of the observed binding energy values for Ag3d, Sb3d and S2p agreed with the literature data [12,13]. No obvious impurities could be detected in the sample, indicating that the level of impurities is lower than the resolution limit of XPS (1 at.%). The quantification of the peaks gives a Ag:Sb:S ratio of $Ag_{3.06}SbS_{3.11}$, which is close to the stoichiometry of Ag_3SbS_3.

The morphology and size of the as-synthesized products are characterized by a field-emission scanning electron microscope (FESEM), which can be seen from the Fig. 3; the low-magnification image (Fig. 3a) reveals that typical products consist of large quantity of rod-like structures. Obviously, the high-magnification image (Fig. 3b) shows that the rod-like structures have almost uniform widths of about 150–200 nm and lengths up to several micrometers. The chemical composition of these nanorods is further confirmed by energy dispersive X-ray spectroscopy (EDS) shown in Fig. 3c. Only peaks of the elements Ag, Sb and S are presented in the EDS spectrum. The atomic ratios are calculated to be 42.48:13.93:43.59 by the comparisons of relative areas under

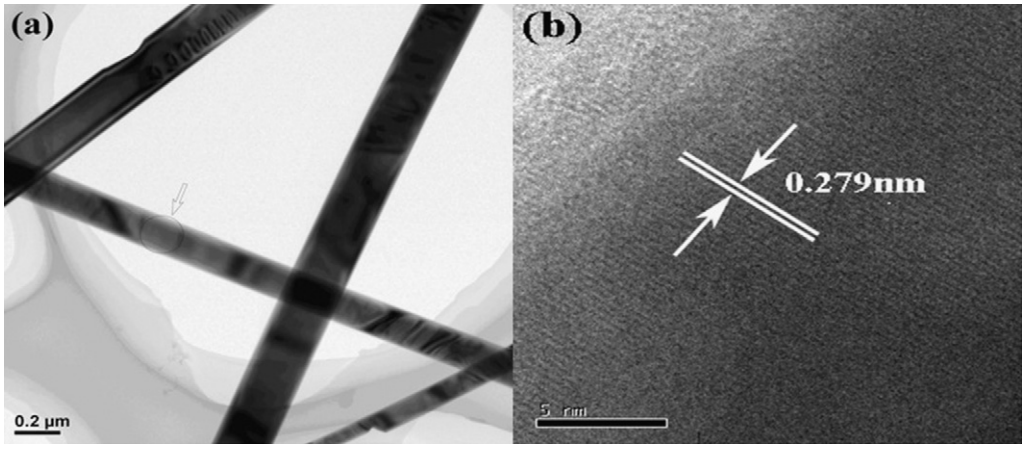

Fig. 4. (a) TEM images of Ag_3SbS_3 nanorods and (b) the corresponding HRTEM pattern taken from the individual Ag_3SbS_3 nanorod. (The HRTEM pattern is obtained from the black circular area demarcated in (a).)

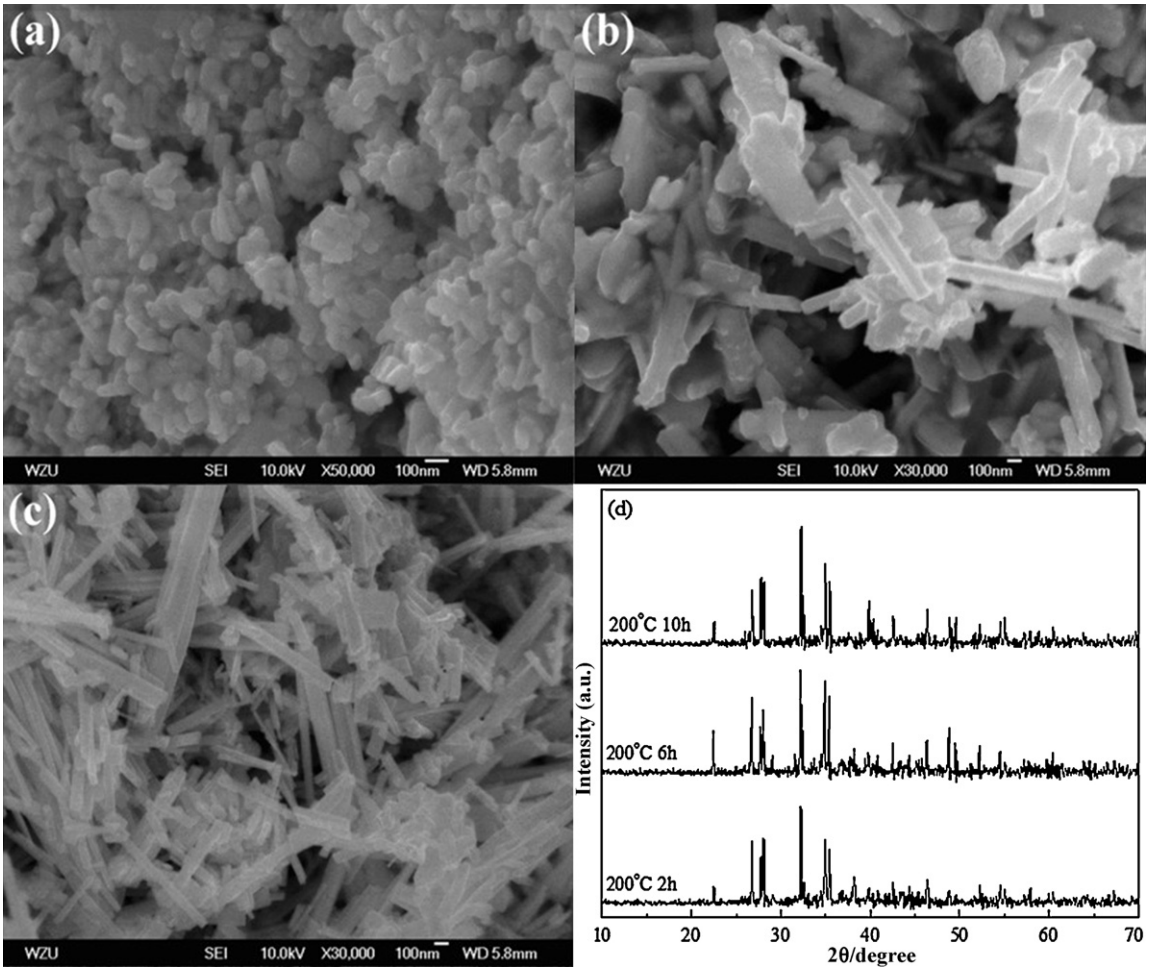

Fig. 5. The FESEM images of Ag_3SbS_3 synthesized at 200 °C for: (a) 2 h, (b) 6 h and (c) 10 h, respectively; (d) XRD patterns of the products synthesized at 200 °C for different reaction times.

the peaks of Ag, Sb and S. This result is consistent with the XRD and XPS pattern presented above.

The structure and morphology of the Ag_3SbS_3 nanostructures are characterized by TEM. Fig. 4a illustrates the TEM image of the prepared Ag_3SbS_3 nanorods. As shown in the image, the product is primarily composed of nanorods with length up to several micrometers and diameter of 100–150 nm. The diameter is very uniform along the entire nanorod. The nanorod is single crystals in nature, which is further confirmed by the HRTEM image presented in Fig. 4b. The distances (0.279 nm) between the adjacent lattice fringes are the interplanar distances of Ag_3SbS_3 (1 2 2) plane, agreeing well with the (1 2 2) d spacing of the literature value of 0.278 nm (JCPDS no. 21-1173).

The influence of temperature and time on the formation of Ag_3SbS_3 is also studied. It is found that Ag_3SbS_3 phase cannot be obtained at a temperature below 170 °C, the unidentified amorphous phases are formed instead. Meanwhile, the crystal phase of Ag_3SbS_3 is unchanged throughout the reaction from 2 to 15 h under 200 °C (Fig. 5d). When the reaction time is 2 h, only irregular Ag_3SbS_3 nanoparticles are obtained (Fig. 5a). When choosing the reaction time to 6 h, the resulting product in Fig. 5b consists of major amount of irregular Ag_3SbS_3 nanoparticles as well as minor amount of rod-like structure are obtained. With the reaction time increasing to 10 h, irregular nanoparticles and short rod-like structure in aggregated states are coexisted in the sample (Fig. 5c). When the reaction time is prolonged to 15 h, a large quantity of nearly uniform rod-like structure is found (Fig. 3a and b). However, varying treatment time from 15 to 24 h at 200 °C did not significantly affect the crystallinity and sizes of the Ag_3SbS_3 nanorods. Thus, for obtaining Ag_3SbS_3 phase with higher crystallinity, the suitable reaction condition is 200 °C and longer than 15 h.

Biomolecules with many functional groups can coordinate with metal cations and form metal–biomolecule complexes, which can serve as precursors of inorganic nanomaterials [26]. Previous literature have reported that antimony ions [27,28] and silver ions [29] could react with amino- and thiol-groups to form complexes. The chemical structure of L-cystine is showed in Fig. 6. In the L-cystine molecule, there are many functional groups, such as $-NH_2$, –COOH, and –SH, which have a strong tendency to coordinate with inorganic cations [15,29] and to form high-affinity metal–biomolecule complexes. In biomolecule-assisted (L-cystine)

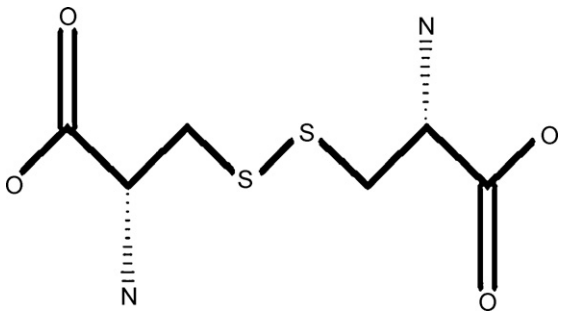

Fig. 6. Chemical structure of L-cystine.

route to Ag_3SbS_3 phase, in the first instance, the preparation of solution of $AgNO_3$–(L-cystine) and $SbCl_3$–(L-cystine) is a key factor to form Ag_3SbS_3 phase. When the three solutions containing $AgNO_3$, $SbCl_3$ and L-cystine are mixed together under constant stirring, a purple floccule occurs simultaneously, which perhaps means the formation of $[Ag(\text{L-cystine})_n]^+$ and $[Sb(\text{L-cystine})_n]^{3+}$ complexes through the combination between silver cation and antimony and the thiol chain. In the following process, the coordinate bond among L-cystine and Sb^{3+} and Ag^+ ruptures when the reaction temperature become higher (200 °C). On the basis of these reports, we propose a mechanism for the formation of Ag_3SbS_3 nanorods. The reactions taking place in the system can be described as follows:

$$Ag^+ + n\text{L-cystine} \xrightarrow{\text{coordination}} [Ag(\text{L-cystine})_n]^+ \quad (1)$$

$$Sb^{3+} + n\text{L-cystine} \xrightarrow{\text{coordination}} [Sb(\text{L-cystine})_n]^{3+} \quad (2)$$

$$[Ag(\text{L-cystine})_n]^+ + [Sb(\text{L-cystine})_n]^{3+} \xrightarrow{\text{decomposition}} Ag_3SbS_3 \quad (3)$$

First, Ag^+ and Sb^{3+} can complex with L-cystine molecules to form $[Ag(\text{L-cystine})_n]^+$ and $[Sb(\text{L-cystine})_n]^{3+}$ complexes in the solution, respectively. The process will not produce large number of free dissociative S^{2-}, Ag^+, and Sb^{3+}, which can prevent the formation of Ag_2S, Sb_2S_3 in the solution. Second, at a suitable temperature, the $[Ag(\text{L-cystine})_n]^+$ and $[Sb(\text{L-cystine})_n]^{3+}$ undergo thermal decomposition to produce Ag_3SbS_3 nanorods. At this stage, due to the relative stability of the complexes, decomposition will proceed more slowly and produce a smaller number of nuclei in the solution than the direct ion-exchange reaction [30]. After rupturing, two forms of nanostructures (nanorods and nanoparticles) coexisted in the solution. When this solution is continuously heated at 200 °C, the small nanoparticles would spontaneously dissolved into the solution due to a relatively higher free energy comparing to nanorods, and the growth units in the solution would diffuse onto the high-energy surface of the growing nanorods [31]. Until the reaction continues for 15 h, uniform nanorods would form eventually. And at the same time, the boiling ethylene glycol makes these newly formed nuclei mix homogeneously, which may promote the oriented growth of the nanorods [30,32]. However, the exact formation mechanism for Ag_3SbS_3 nanorods is still obscure and more studies are in underway.

4. Conclusions

A novel biomolecule-assisted route was proposed for synthesizing the mineral pyrargyrite (Ag_3SbS_3) nanorods using L-cystine as the sulfide source and complexing agent. In this process, the formation of metal–biomolecule complexes ($[Ag(\text{L-cystine})_n]^+$ and $[Sb(\text{L-cystine})_n]^{3+}$) and thermal decomposition were attributed to the formation of Ag_3SbS_3 nanorods. And the reaction time played an important role in the formation of Ag_3SbS_3 nanocrystalline. Crystal structure and composition of product were characterized by XRD, EDS and XPS, morphologies of the product were identified by FESEM and TEM, from which it indicates that diameters of the nanorods are approximate 150–200 nm and lengths up to several micrometers.

Acknowledgment

The authors acknowledge the financial support from National Natural Sciences Foundation of China (Grant nos. 50772075 and 50972107).

References

[1] N. Herron, Y. Wang, H. Eckert, J. Am. Chem. Soc. 112 (1990) 1322–1326.
[2] P.F. Yang, B. Song, R. Wu, Y.F. Zheng, Y.F. Sun, J.K. Jian, J. Alloys Compd. 481 (2009) 450–454.
[3] F. Li, W.T. Bi, T. Kong, C.J. Wang, Z. Li, X.T. Huang, J. Alloys Compd. 479 (2009) 707–710.
[4] S. Iijima, Nature 354 (1991) 56–58.
[5] A.M. Morales, C.M. Lieber, Science 279 (1998) 208–211.
[6] H.M. Wang, Z. Chen, Q. Cheng, L.X. Yuan, J. Alloys Compd. 478 (2009) 872–875.
[7] L.K. Samanta, S. Chatterjee, Phys. Status Solidi B 182 (1994) 85–89.
[8] S.A. Aliev, S.S. Ragimov, Neorg. Mater. 28 (1992) 329–334.
[9] H. Tang, J.G. Yu, X.F. Zhao, J. Alloys Compd. 460 (2008) 513–518.
[10] L. Panchenko, H. Khlyap, V. Laptev, Appl. Surf. Sci. 255 (2009) 5256–5259.
[11] D. Adler, M.S. Shur, M. Silver, S.R. Ovchinsky, J. Appl. Phys. 51 (1980) 3289–3309.
[12] H.L. Su, Y. Xie, S.K. Wan, B. Li, Y.T. Qian, Solid State Ionics 123 (1999) 319–324.
[13] D. Chen, G.Z. Shen, K.B. Tang, X. Jiang, L.Y. Huang, Y. Jin, Y.T. Qian, Mater. Res. Bull. 38 (2003) 509–513.
[14] W. Fritzsche, K.J. Böhm, E. Unger, J.M. Köhler, Appl. Phys. Lett. 75 (1999) 2854–2856.
[15] F. Zuo, S. Yan, B. Zhang, Y. Zhao, Y. Xie, J. Phys. Chem. C 112 (2008) 2831–2835.
[16] L.Q. Dong, T. Hollis, B.A. Connolly, N.G. Wright, B.R. Horrocks, A. Houlton, Adv. Mater. 19 (2007) 1748–1751.
[17] R.A. McMillan, J. Howard, N.J. Zaluzec, H.K. Kagawa, R. Mogul, Y.F. Li, C.D. Paavola, J.D. Trent, J. Am. Chem. Soc. 127 (2005) 2800–2801.
[18] Q. Lu, Y.F. Gao, S. Komarneni, J. Am. Chem. Soc. 126 (2004) 54–55.
[19] J.Q. Jiao, X. Liu, W. Gao, C.W. Wang, H.J. Feng, X.L. Zhao, L.P. Chen, Solid State Sci. 11 (2009) 976–981.
[20] C. Radloff, R.A. Vaia, J. Brunton, G.T. Bouwer, V.K. Ward, Nano. Lett. 5 (2005) 1187–1191.
[21] X.F. Yang, X.T. Dong, J.X. Wang, G.X. Liu, Mater. Lett. 63 (2009) 629–631.
[22] B. Zhang, X.C. Ye, W. Dai, W.Y. Hou, F. Zuo, Y. Xie, Nanotechnology 17 (2006) 385–390.
[23] Y.Q. Lei, S.Y. Song, W.Q. Fan, Y. Xing, H.J. Zhang, J. Phys. Chem. C 113 (2009) 1280–1285.
[24] Y.L. Min, Y.C. Chen, Y.G. Zhao, Solid State Sci. 11 (2009) 451–455.
[25] J.H. Jiang, R.M. Yu, J.Y. Zhu, R. Yi, G.Z. Qiu, Y.H. He, X.H. Liu, Mater. Chem. Phys. 115 (2009) 502–506.
[26] J.H. Xiang, H.Q. Cao, Q.Z. Wu, S.C. Zhang, X.R. Zhang, Cryst. Growth Des. 8 (2008) 3935–3940.
[27] X.Y. Chen, X.F. Zhang, C.W. Shi, X.L. Li, Y.T. Qian, Solid State Commun. 134 (2005) 613–615.
[28] Z.J. Zhang, X.Y. Chen, J. Phys. Chem. Solids 70 (2009) 1121–1131.
[29] J.H. Xiang, H.Q. Cao, Q.Z. Wu, S.C. Zhang, X.R. Zhang, A.A.R. Watt, J. Phys. Chem. C 112 (2008) 3580–3584.
[30] J.Q. Hu, B. Deng, W.X. Zhang, K.B. Tang, Y.T. Qian, Int. J. Inorg. Mater. 3 (2001) 639–642.
[31] Z.P. Liu, D. Xu, J.B. Liang, W.J. Lin, W.C. Yu, Y.T. Qian, J. Solid State Chem. 178 (2005) 950–955.
[32] G.Z. Shen, D. Chen, K.B. Tang, Y.T. Qian, J. Cryst. Growth 252 (2003) 199–201.